Article:
Asker, A., Omar, M., Zhang, J. et al. (3 more authors) (2025) Optimum Design of Polycentric Knee Hinges Based on Analysis of Knee-exoskeleton Closed Kinematic Chain. Proceedings of the Institution of Mechanical Engineers, Part C: Journal of Mechanical Engineering Science. ISSN 0954-4062

https://doi.org/10.1177/09544062251313926

Optimum Design of Polycentric Knee Hinges Based on Analysis of Knee-exoskeleton Closed Kinematic Chain

Ahmed Asker[1,2], Mohamed Omar[2,3], Junyang Zhang[3], Ke Wang[3], Ruifeng Li[3] and Shengquan Xie[4]

Abstract

Knee exoskeletons are devices that can enhance users' mobility and strength. Their compatibility with the user's joint motion is crucial for proper functioning. Typically, knee hinges are designed to replicate the instantaneous center of rotation (ICR) of an average knee. This study represents a knee exoskeleton worn by a user as 1 DoF closed-kinematic chain, which enables calculating the displacement between the exoskeleton and the user's thigh. The problem of optimizing the exoskeleton hinges to yield low relative movements during flexion and extension motions is formulated based on the proposed analysis. Also, the 4-bar knee model was simulated with different exoskeleton hinge designs to demonstrate the ability of the proposed analysis to predict the relative motions under different alignment conditions. The performance of an optimized polycentric geared knee hinge is then compared experimentally with that of a typical fixed center hinge. Experimental results showed that the optimized polycentric hinge yields less relative motion and a lower chance of exoskeleton migration. The proposed method emphasizes the importance of minimizing relative motion rather than replicating the knee's ICR and provides a systematic way to design and evaluate various knee hinge designs.

Keywords

Knee Exoskeleton Design, Polycentric Knee Joint, Knee Motion Kinematics, Optimum Knee Joint Design.

Introduction

Knee joints have a complex structure, which plays a vital role in weight-bearing, ambulation, and stability[1,2]. Knee dysfunction has a significant implication for mobility and has a negative impact on quality of life, preventing affected people from enjoying their lives. For example, the incapacity to generate sufficient knee torque needed for high-weight-bearing activities such as sit-to-stand can significantly affect the ability to independently perform activities of daily living[3]. Various injuries and diseases can affect knee function. Knee injuries are quite common and account for about 60% of all sports injuries[4]. Ligaments and meniscus tears are the most prevailing knee injuries. Also, diseases such as osteoarthritis are common, especially among senior citizens.

The human knee has 6 DoF complex motion kinematics, which involves flexion/extension, abduction/adduction, and internal/external rotation[5]. The main knee joint motion is the rotation in the sagittal plane (flexion/extension), which has an active range of about 120°[6]. There are various approaches to modeling knee joints, from simply describing their movement in the sagittal plane to creating detailed models that include the bones, muscles, tendons, and ligaments involved in the joint's motion[7,8]. Furthermore, other studies have investigated the effect of weight-bearing on knee kinematics[6,9,10].

In this study, we are interested in models that describe knee motion kinematics only. The geometry of the cruciate ligaments and the articular surfaces in the tibiofemoral joint can be used to model the motion of the knee in the sagittal plane as presented in[11]. This model assumes that the cruciate ligaments behave as two inextensible fibers (rigid links) that cross each other at the instantaneous center of rotation (ICR) of the knee[12]. Together with the femur and tibia bones, they form a crossed 4-bar mechanism (4-BM). Only 2-D motion is considered in this model, while the knee motion has 6 DoFs. Generally, the 2D models did not consider the knee's flexion and extension axes offset from the anatomic sagittal plane or the concurrent longitudinal rotation around an axis separate from the knee's flexion and extension axes. Despite that, the 4-BM was supported by many studies[13] and can accurately approximate the motion of the knee in the sagittal plane[14]. Magnetic resonance imaging (MRI) has significantly advanced the study of

[1]Smart Engineering Systems Research Center (SESC), School of Engineering & applied science, Nile University, Giza, Egypt
[2]Department of production engineering and mechanical design, Faculty of Engineering, Mansoura University, Mansoura, Egypt.
[3]State Key Laboratory of Robotics and System, Harbin Institute of Technology, China
[4]School of Electronic and Electrical Engineering, Faculty of Engineering, University of Leeds, UK

Corresponding author:
Ahmed Asker, Department of production engineering and mechanical design, Faculty of Engineering, Mansoura University, Mansoura, Egypt.
Email: a_askar@mans.edu.eg

knee kinematics by enabling precise 3D analysis of the knee. Numerous studies have focused on using MRI to describe the motion kinematics of the normal knee[1,6,9,10]. That leads to a fundamental revision of knee kinematics, which boosts understanding of how knee pathology affects motion kinematics[15]. Walker et al.[16] studied the motion of 14 cadavers and 8 volunteers to obtain the relationship between knee kinematics and flexion angle. The posterior parts of the femoral condyles were modeled as spheres, which were projected in the sagittal plane by radiography as circles with center points coincident with the posterior spheres. The axis of the system was constructed by connecting the centers of the circles, which defined a 3D model of the femur orientation on the tibia. A model of an average knee was obtained, which could be scaled to represent a particular user knee. This model was further refined in[17] and is widely used to design external knee hinges[18–21].

Minimizing misalignment between a knee hinge and the user's knee is an essential design criterion, as misalignment can cause discomfort or injury due to unwanted forces at the skin-cuff interface[22]. Several techniques have been proposed in the literature to address this issue, including:

- **Manual alignment** is the most common method for aligning a knee hinge. It is done by the practitioner manually adjusting the hinge until the misalignment is minimized. However, this method is time-consuming and error-prone[23].
- **Polycentric knee hinges** have multiple axes of rotation, which allows the ICR of the biological and external knee to be as close as possible. This reduces the misalignment between the two joints and minimizes the unwanted forces at the skin-cuff interface[24].
- **Self-aligning knee hinges** can adjust their center of rotation to accommodate any misalignment. This is done using a passive or active joints that allows the hinge to follow the complex motion of the knee joint[25,26].

The most basic hinge design can be realized by assuming a fixed center of rotation for the knee joint. This design is susceptible to misalignment due to oversimplified joint kinematics and inaccurate fit or positioning. Misalignment always occurs and increases with the flexion angle, which requires frequent realignments due to brace/exoskeleton migration[27].

Designing a hinge compatible with the motion of the human knee can be achieved by different design approaches such as multi-link, cam, geared, or compliant mechanisms hinges. There are two main methods for designing multi-link knee hinges. The first method is to design a multi-link mechanism such that the ICR of the link attached to the human thigh coincides with the ICR of the human knee. This design assumes a rigid connection between the lower limbs and the brace/exoskeleton and ignores the viscoelasticity of human tissues[28]. The design is formulated as an optimization problem of finding the mechanism parameters that minimize the difference between the hinge and knee ICR. Intra-subject and inter-subject variability affect the accuracy of the kinematic model of the human knee, thus, discrepancies between the biological and exoskeleton joints are unavoidable. This results in an overconstrained closed-kinematic chain when attached to the lower limbs[29]. The second approach is to design a self-aligning mechanism such as Schmidt coupling[30] or 3-RRP mechanism[31]. Adding passive DoFs to achieve self-alignment increases design complexity and increases hinge inertia[30,31]. Cam mechanisms[16] are designed such that the cam profile replicates the locus of the ICR of the human knee. Cam mechanisms have the same limitations as multi-link joints. In addition, they have a complex profile and are subject to wear and tear due to the sliding contact. The geared knee hinge consists of two meshed gears with a movable link connected to the centers of the two gears by revolute joints, which give it planetary motion. Compliant mechanisms[32] and soft material can comply with the joint kinematics motion, but their deformability limits the force they can support. Compliant elements can only accommodate small misalignment[33] as they produce a reaction torque around the joint proportional to its deformation.

This study was motivated by our experience with three different knee hinge designs: fixed center, polycentric geared and polycentric 5-bar[34] (Figure 1). The fixed center knee hinge Figure 1a, which the most common in the market showed an appreciable misalignment and brace/exoskeleton migration, which increased with knee flexion angle. This misalignment would need to be corrected regularly to ensure proper function. The polycentric geared knee hinge Figure 1b properly aligns with the user's knee at low flexion angles, but it experiences a noticeable misalignment near full flexion. These observations are not new, and similar results have been reported in previous studies[35,36]. For example, in[35], an experiment compared three knee brace designs: fixed center, geared, and geared with a self-aligning center of rotation hinge. The self-aligning hinge showed significantly less migration than the fixed center and geared hinges. Additionally, the study in[36] demonstrated that multi-link mechanisms with passive joints can follow knee motion and reduce relative movements.

The polycentric 5-bar hinge Figure 1c was optimized in[34] to reduce the Euclidean distance between the ICR of the mechanism and that of an average knee presented in[17]. It effectively followed the knee motion from full extension to deep squat. However, the 5-bar hinge is quite bulky and more expensive to manufacture relative to geared hinges. Most of the design approaches found in the literature depend on replicating the ICR of an average knee. This design approach is very restrictive, as any misalignment would result in an overdetermined knee-exoskeleton closed-kinematic chain (K-E CKC)[29]. The geared hinge has the potential to provide a compact hinge design due to its simplicity, but an efficient design method is needed because its ICR is much different than that of the knee. Also, an analysis method is needed to model the relative motion between exoskeletons and the user's leg for various knee hinge designs, especially when misalignment occurs.

This paper introduces a new approach to studying and designing knee hinges that consider the kinematics of the human knee and the exoskeleton hinge. The paper assumes that the user's leg can be represented by rigid links as presented in[25,28,36]. As the motion between the user's leg and the exoskeleton is inevitable, connecting them yields

(a) (b) (c)

Figure 1. A subject tries knee braces with different hinge designs at knee extension and deep knee squat (a) fixed center, (b) polycentric geared, and (c) polycentric 5-bar.

an overconstrained structure if they are rigidly attached to each other[29,37]. In this study, it is assumed that the knee hinge and the user's leg create two kinematic chains, which are joined in a way that results in a kinematic chain with 1 DoF in the Sagittal plane, where the flexion and extension motions occur. That simplifies the kinematic analysis of the relative motion between the brace/exoskeleton and the user's leg. Also, the proposed approach can be used to optimize the design of various knee hinge designs.

The rest of the paper is organized as follows: the next section models the human knee kinematics based on the 4-BM. This is followed by an analysis of knee-exoskeleton kinematics as a closed-kinematic chain. The proposed analysis is then used to optimize various knee hinge designs. In the subsequent section, different knee hinge designs are simulated. An experiment is conducted in the next section to compare the fixed center and optimized geared hinges. Finally, the last two sections discuss the results and provide the conclusion.

Modeling of human knee kinematic

This section briefly describes the knee motion model of adults described in[17] and presents the kinematic analysis of the 4-BM knee models.

Model of human knee ICR

The knee varus rotation, R_V, internal rotation, R_I, proximal-distal translation, D_{PD}, and anterior-posterior translation, D_{AP}, were obtained as a function of the knee flexion angle, θ_{kf} for $\theta_{kf} \in [0° \quad 120°]$ as follow[17]:

$$R_V = 0.0791\theta_{kf} - 5.733 \times 10^{-4}\theta_{kf}^2 - 7.682 \times 10^{-6}\theta_{kf}^3 + 5.759 \times 10^{-8}\theta_{kf}^4$$

$$R_I = 0.3695\theta_{kf} - 2.958 \times 10^{-3}\theta_{kf}^2 + 7.666 \times 10^{-6}\theta_{kf}^3$$

$$D_{PD} = -0.0683\theta_{kf} + 8.804E-4\theta_{kf}^2 - 3.750 \times 10^{-6}\theta_{kf}^3$$

$$D_{AP} = -0.1283\theta_{kf} + 4.796 \times 10^{-4}\theta_{kf}^2$$

The ICR position (z_k, y_k) of the knee in the sagittal plane ($z_k y_k$ plane), can be described as a function of knee varus rotation, R_V, internal rotation, R_I, proximal-distal translation, D_{PD}, and anterior-posterior translation, D_{AP}[17] as follows:

$$\begin{bmatrix} z_k \\ y_k \end{bmatrix} = \begin{bmatrix} -\sin(R_V)x_k + D_{PD} \\ \cos(R_V)\sin(R_I)x_k + D_{AP} \end{bmatrix} \quad (1)$$

where x_k is the lateral distance in mm measured from frame $O_k x_k y_k z_k$ as shown in Figure 2a. It is assumed that the exoskeleton is laterally attached to the user's leg at a distance $x_k = -60mm$ as reported in[38]. Figure 2b shows the locus of the knee ICR in the $z_k y_k$ plane at $x_k = -60mm$.

Kinematic analysis of 4-BM model of human knee

The schematic of the 4-BM representation of human knee is shown in Figure 2c. This model has only 1 Dof which enables flexion and extension in the sagittal plane. The shank link (Figure 2c) is assumed to be stationary and the knee flexion is achieved by the rotation of link $k3$ (Femur) relative to link $k1$ (shank).In all of the following analyses, the length of link ji and its angle of rotation about x_{k2} axis are denoted as l_{ji} and θ_{ji} respectively, where:

$$j = \begin{cases} k & \text{for knee 4-BM model} \\ e & \text{for exoskeleton} \end{cases}$$

Also, we assume at zero flexion angle ($\theta_{kf} = 0$) that $\theta_{ji} = \alpha_{ji}$, where α_{ji} can be obtained graphically by plotting the corresponding linkage at $\theta_{kf} = 0$.

To obtain the angle of the moving links as a function of θ_{kf}, the closed chain $O_{k2}ABO_{k4}O_{k2}$ is written in the vector form as follows:

$$\overrightarrow{O_{k2}A} + \overrightarrow{AB} - \overrightarrow{O_{k4}B} - \overrightarrow{O_{k2}O_{k4}} = 0 \quad (2)$$

The horizontal and vertical components of equation (2) can be written as follows:

$$l_{k2}\cos\theta_{k2} + l_{k3}\cos\theta_{k3} - l_{k4}\cos\theta_{k4} - l_{k1}\cos\theta_{k1} = 0 \quad (3)$$

$$l_{k2}\sin\theta_{k2} + l_{k3}\sin\theta_{k3} - l_{k4}\sin\theta_{k4} - l_{k1}\sin\theta_{k1} = 0 \quad (4)$$

For a given θ_{kf}, the following relations can be deduced from Figure 2c:

$$\theta_{k3} = (\theta_{kf} + \alpha_{k3}) - \frac{\pi}{2} \quad (5)$$

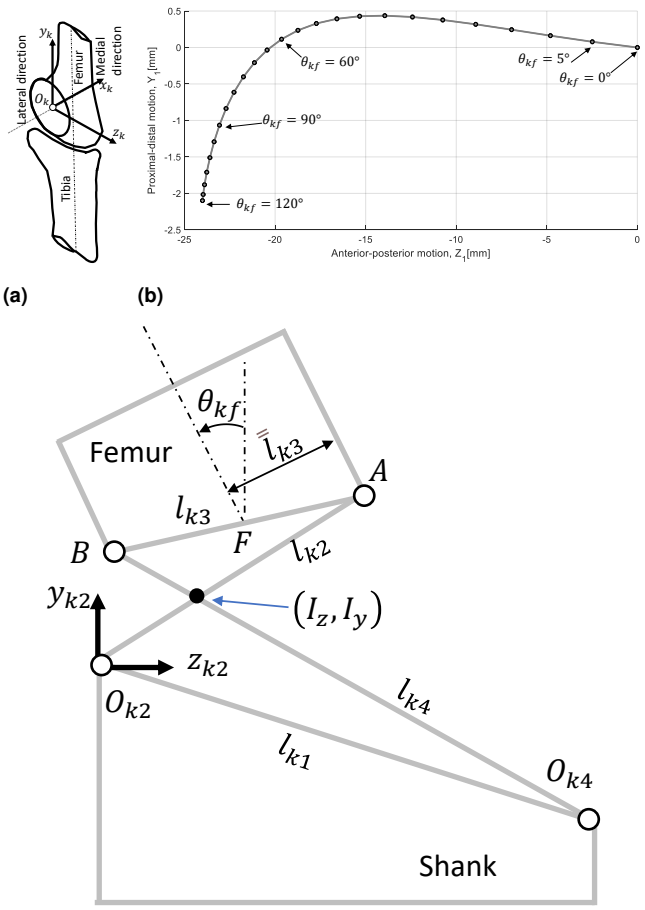

Figure 2. Knee motion Kinematics (a) knee reference coordinate frame, (b) Proximal-distal and anterior-posterior motions of the knee ICR at $x_k = -60mm$, and (c) the 4-BM model of the knee.

Thus, equation (3) and equation (4) can be easily solved for θ_{k2} and θ_{k4} using the same approach presented in [39], that yields the following:

$$\theta_{k2} = 2atan2(-\eta_1 \pm \sqrt{\eta_1^2 + \eta_2^2 - \eta_3^2}\,, \eta_3 - \eta_2) \qquad (6)$$

$$\theta_{k4} = 2atan2(-\zeta_1 \pm \sqrt{\zeta_1^2 + \zeta_2^2 - \zeta_3^2}, \zeta_3 - \zeta_2) \qquad (7)$$

where

$$\begin{aligned}
\eta_1 &= -2l_{k2}\left(l_{k1}\sin\theta_{k1} - l_{k3}\sin\theta_{k3}\right),\\
\eta_2 &= -2l_{k2}\left(l_{k1}\cos\theta_{k1} - l_{k3}\cos\theta_{k3}\right),\\
\eta_3 &= l_{k1}^2 + l_{k2}^2 + l_{k3}^2 - l_{k4}^2 - 2l_{k1}l_{k3}\,cos(\theta_{k1} - \theta_{k3}),\\
\zeta_1 &= 2l_{k4}\left(l_{k1}\sin\theta_{k1} - \ l_{k3}\sin\theta_{k3}\right),\\
\zeta_2 &= 2l_{k4}\left(l_{k1}\cos\theta_{k1} - l_{k3}\cos\theta_{k3}\right),\\
\zeta_3 &= l_{k1}^2 - l_{k2}^2 + l_{k3}^2 + l_{k4}^2 - 2l_{k1}l_{k3}\,cos(\theta_{k1} - \theta_{k3})
\end{aligned}$$

The location of the crossed 4-BM ICR, (I_z, I_y), shown in Figure 2c is located at the intersection of line $O_{k2}A$ with line $Q_{k4}B$, which can be obtained relative to the $O_{k2}z_ky_k$ coordinate frame as follows:

$$\begin{bmatrix} I_z \\ I_y \end{bmatrix} = \begin{bmatrix} \frac{O_{k4y}}{m_1 - m_2} - \frac{O_{k4z}\,m_2}{m_1 - m_2} \\ \frac{O_{k4y}\,m_1}{m_1 - m_2} - \frac{O_{k4z}\,m_1\,m_2}{m_1 - m_2} \end{bmatrix} \qquad (8)$$

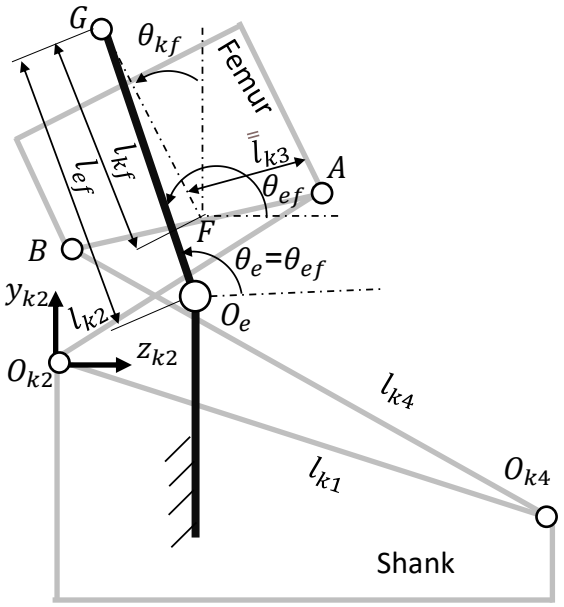

Figure 3. Schematic of the 4-BM knee model with fixed center knee brace.

in which

$$m_1 = \frac{A_y}{A_z}, \qquad m_2 = \frac{B_y - O_{k4y}}{B_z - O_{k4z}}$$

where (A_z, A_y), (B_z, B_y) and (O_{k4z}, O_{k4y}) are the position of points A, B and O_{k4} relative to $O_{k2}z_ky_k$ coordinate frame, respectively.

Kinematic analysis of Knee-exoskeleton Closed-Kinematic Chain

In this section, the kinematics of the K-E CKC are analyzed to obtain the sliding and torsional deviations between the exoskeleton and the user's thigh. The exoskeleton is assumed to be rigidly attached to the shank link and connected to the thigh link by a 2 DoF joint (allow both translation and rotation similar to pin-in-slot joint), which enables relative linear and rotational motion between the users thigh and the exoskeleton.

At $\theta_{kf} = 0°$, the distance between the ICR of the knee 4-BM model and the point of contact between the exoskeleton and user's thigh is fixed by the exoskeleton design. In this paper we assume that $l_{ef} = 10\ cm$ (Figure 3 through 5). Also, the angle α_{ij} of the different links can be obtained graphically.

In the next analyses, it is assumed that θ_{ki} for $i = 2, 3, 4$ have been already obtained from equations (5), (6) and (7).

Fixed-center hinge

The kinematic analysis of the K-E CKC shown in Figure 3 can be preformed by writing the closed loop $O_{k2}AFGO_eO_{k2}$ in the vector form as follows:

$$\overrightarrow{O_{k2}A} + \overrightarrow{AF} + \overrightarrow{FG} - \overrightarrow{O_eG} - \overrightarrow{O_{k2}O_e} = 0 \qquad (9)$$

The components of equation (9) can be written as follows:

$$l_{k2}\cos\theta_{k2} + \bar{\bar{l}}_{k3}\cos\theta_{k3} + l_{kf}\cos\theta_{kf} - l_{ef}\cos\theta_e - O_{ez} = 0 \qquad (10)$$

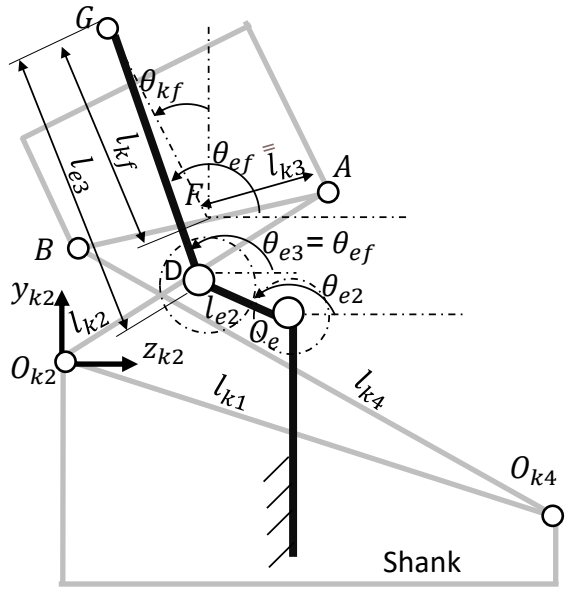

Figure 4. Schematic of the 4-BM knee model with polycentric geared knee brace.

$$l_{k2}\sin\theta_{k2}+\bar{\bar{l}}_{k3}\sin\theta_{k3}+l_{kf}\sin\theta_{kf}-l_{ef}\sin\theta_e-O_{ey}=0 \tag{11}$$

It can be noted that, for a θ_{kf}, equation (10) and equation (11) can be solved for l_{kf} and θ_e as follows:

$$l_{kf}=\frac{-b\pm\sqrt{b^2-4c}}{2} \tag{12}$$

$$\begin{aligned}\theta_e =& atan2(l_{k2}\sin\theta_{k2}+\bar{\bar{l}}_{k3}\sin\theta_{k3}+l_{kf}\sin\theta_{kf}-\\ & O_{ey}, l_{k2}\cos\theta_{k2}+\bar{\bar{l}}_{k3}\cos\theta_{k3}+l_{kf}\cos\theta_{kf}-O_{ez})\end{aligned} \tag{13}$$

where

$$\begin{aligned}b=&2\bar{\bar{l}}_{k3}\cos(\theta_{k3}-\theta_{kf})-2(O_{ey}\sin\theta_{kf})-2(O_{ez}\cos\theta_{kf})\\ &+2l_{k2}\cos(\theta_{k2}+\theta_{kf})\end{aligned}$$

$$\begin{aligned}c=&O_{ey}^2+O_{ez}^2+l_{k2}^2-l_{ef}^2+(l'_{k3})^2-2\bar{\bar{l}}_{k3}O_{ey}\sin\theta_{k3}\\ &-2l_{k2}O_{ey}\sin\theta_{k2}-2\bar{\bar{l}}_{k3}O_{ez}\cos\theta_{k3}-2l_{k2}O_{ez}\cos\theta_{k2}\\ &+2\bar{\bar{l}}_{k3}l_{k2}\cos(\theta_{k2}-\theta_{k3})\end{aligned}$$

in which, O_{ez} and O_{ey} is the horizontal and vertical component of point O_e relative to $O_{k2}z_{k2}y_{k2}$ coordinate frame.

The value of $\bar{\bar{l}}_{k3}$ can be obtained by assuming that at $\theta_{kf}=0$, the hinge center is aligned with the ICR of the 4-BM model of the knee (Figure 3) and point F lies on the line $O_e\,G$. That yields the following:

$$\bar{\bar{l}}_{k3}=\frac{O_{ez}-l_{k2}\cos(\alpha_{k2})}{\cos(\alpha_{k3})} \tag{14}$$

Geared hinge

The kinematic analysis of the K-E CKC shown in Figure 4 can be preformed by writing the closed loop $O_{k2}AFGDO_eO_{k2}$ in the vector form as follows:

$$\overrightarrow{O_{k2}A}+\overrightarrow{AF}+\overrightarrow{FG}-\overrightarrow{DG}-\overrightarrow{O_eG}-\overrightarrow{O_{k2}O_e}=0 \tag{15}$$

The components of equation (15), can be written as follows:

$$\begin{aligned}&O_{ez}+l_{e2}\cos\theta_{e2}+l_{e3}\cos\theta_{e3}-l_{kf}\cos\theta_{kf}\\ &-\bar{\bar{l}}_{k3}\cos\theta_{k3}-l_{k2}\cos\theta_{k2}=0.\end{aligned} \tag{16}$$

$$\begin{aligned}&O_{ey}+l_{e2}\sin\theta_{e2}+l_{e3}\sin\theta_{e3}+-l_{kf}\sin\theta_{kf}\\ &-\bar{\bar{l}}_{k3}\sin\theta_{k3}-l_{k2}\sin\theta_{k2}=0\end{aligned} \tag{17}$$

where

$$\theta_{e3}=\left(\frac{r_1+r_3}{r_3}\right)(\theta_{e2}-\alpha_{e2})+\alpha_{e3}$$

$$l_{e2}=r_1+r_3$$

Referring to Figure 4 and assuming at $\theta_{kf}=0$, the hinge center is aligned with the ICR of 4-BM knee model and point F lies on the line DG, $\bar{\bar{l}}_{k3}$ can be obtained as follows:

$$\bar{\bar{l}}_{k3}=\frac{O_{ez}+l_{e2}\cos(\alpha_{e2})-l_{k2}\cos(\alpha_{k2})}{\cos(\alpha_{k3})}$$

The length of the exoskeleton link connected to the user's thigh can be obtained as follows:

$$l_{e3}=\frac{I_{y0}+l_{ef}-O_{ey}-l_{e2}\sin(\alpha_{e2})}{\sin(\alpha_{e3})}$$

where I_{y0} and l_{ef} are the vertical position of the knee ICR at $\theta_{kf}=0$ relative to $O_{k2}z_{k2}y_{k2}$ coordinate frame and the vertical distance between point G and the the knee ICR at $\theta_{kf}=0$.

The value of l_{kf} and θ_{e2} can be obtained by solving equations (16) and (17) numerically. The value of l_{kf} and θ_{e2} at $\theta_{kf}=0$ is obtained graphically, then the solution is obtained numerically using MATLAB *fsolve* function for $\theta_{kf}=i\Delta\theta_{kf};\ i=1,2,\ldots,N$, where N, $\Delta\theta_{kf}=\frac{(\theta_{kf})_{\max}}{N}$ and $(\theta_{kf})_{\max}$ are the number of solution points, increment of the flexion angle and maximum flexion angle, respectively. To enhance the numerical convergence the solution at point $i-1$ is set as the initial point for solving at point i.

4-BM knee hinge

The vector equation of the closed loop $O_{k2}AFGDO_{e2}O_{k2}$ shown in Figure 5 can be written as follows:

$$\overrightarrow{O_{k2}A}+\overrightarrow{AF}+\overrightarrow{FG}-\overrightarrow{HG}-\overrightarrow{PH}-\overrightarrow{O_{e2}P}-\overrightarrow{O_{k2}O_{e2}}=0 \tag{18}$$

Writing the horizontal and vertical components of equation (18), that yields:

$$\begin{aligned}&O_{ez}+l_{e2}\cos\theta_{e2}+\bar{\bar{l}}_{e3}\cos\theta_{e3}+l_{ef}\cos\theta_{ef}\\ &-l_{kf}\cos\theta_{kf}-\bar{\bar{l}}_{k3}\cos\theta_{k3}-l_{k2}\cos\theta_{k2}=0\end{aligned} \tag{19}$$

$$\begin{aligned}&O_{ey}+l_{e2}\sin\theta_{e2}+\bar{\bar{l}}_{e3}\sin\theta_{e3}+l_{ef}\sin\theta_{ef}\\ &-l_{kf}\sin\theta_{kf}-\bar{\bar{l}}_{k3}\sin\theta_{k3}-l_{k2}\sin\theta_{k2}=0\end{aligned} \tag{20}$$

where

$$\theta_{ef}=\theta_{e3}-\alpha_{e3}+\frac{\pi}{2}$$

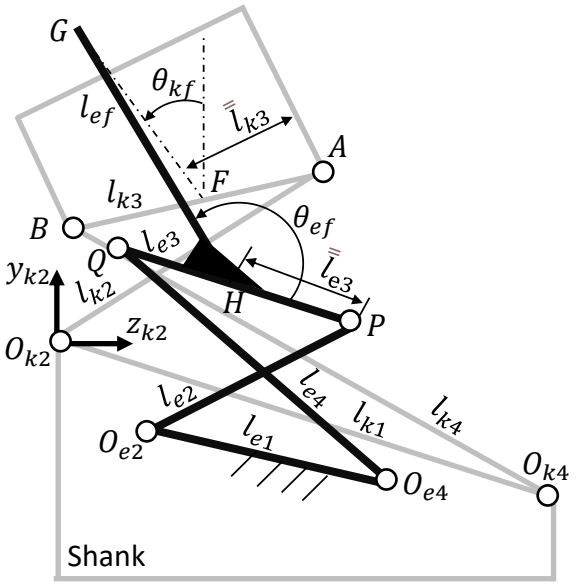

Figure 5. Schematic of the 4-BM knee model with polycentric 4-BM knee brace.

The closed loop vector equation in equation (19) and equation (20) contains three unknowns. Thus, another loop equation should be used. The closed loop $O_{e2}PQO_{e4}O_{e2}$ can be written in the vector form as follows:

$$\overrightarrow{O_{e2}P} + \overrightarrow{PQ} - \overrightarrow{O_{e4}Q} - \overrightarrow{O_{e2}O_{e4}} = 0 \tag{21}$$

Similarly, the components of equation (21) is as follows:

$$-l_{e1}\cos\theta_{e1} + l_{e2}\cos\theta_{e2} + l_{e3}\cos\theta_{e3} - l_{e4}\cos\theta_{e4} = 0 \tag{22}$$

$$-l_{e1}\sin\theta_{e1} + l_{e2}\sin\theta_{e2} + l_{e3}\sin\theta_{e3} - l_{e4}\sin\theta_{e4} = 0 \tag{23}$$

Referring to Figure 5 the following equations can be obtained:

$$l_{ef} = \frac{I_{y0} + l_{ef} - O_{ey} - l_{e2}\sin(\alpha_{e2}) - \bar{\bar{l}}_{e3}\sin\alpha_{e3}}{\sin(\alpha_{ef})}$$

$$\bar{\bar{l}}_{k3} = \frac{O_{ez} + l_{e2}\cos(\alpha_{e2}) + \bar{\bar{l}}_{e3}\cos(\alpha_{e3}) - l_{k2}\cos(\alpha_{k2})}{\cos(\alpha_{k3})}$$

Assuming at $\theta_{kf} = 0$, the exoskeleton link HG is vertical and point H is the midpoint of link $e3$ that yields:

$$\alpha_{ef} = \frac{\pi}{2} \tag{24}$$

$$\bar{\bar{l}}_{e3} = \frac{l_{e3}}{2} \tag{25}$$

Thus, equations (19) through (23) can be numerically solved for $\theta_{e2},\ \theta_{e3}, \theta_{e4}$ and l_{kf}.

Optimization of multi-link knee hinges

In this section, the dimensions of a 4-BM are optimized to replicate the knee motion kinematics (equation (1)). Then, the optimized 4-BM knee model is used to find the dimensions of different knee hinges that minimize the relative motion between the exoskeleton and the thigh link.

Optimal 4-BM knee model

The optimal dimensions of the 4-BM are obtained using the same approach described in[18,39]. The objective is to minimize the Euclidean distance between the ICR of the human knee presented in equation (1) and the ICR of the 4-BM obtained in equation (8). The design vector, χ, is as follows:

$$\chi = [l_{k1}\ l_{k2}\ l_{k3}\ l_{k4}\ O_{k2z}\ O_{k2y}\ \alpha_{k1}\ \alpha_{k3}]^T \tag{26}$$

where $(O_{k2z},\ O_{k2y})$ is the position of frame $O_{k2}z_{k2}y_{k2}$ relative to frame $O_k z_k Y_k$, while α_{k1} and α_{k2} are the value of angles θ_{k1} and θ_{k2} at $\theta_{kf} = 0$.

The cost function can be formulated as follows:

$$C_{4B}(\chi) = \frac{1}{N}\sum_{\theta_{kf}=0}^{\theta_{kf}=120^\circ} \left\| \begin{bmatrix} I_z(\theta_{kf}) - z_k(\theta_{kf}) \\ I_y(\theta_{kf}) - y_k(\theta_{kf}) \end{bmatrix} \right\|_2 \tag{27}$$

where $\|*\|$ is the second norm of the vector $*$ and N is the number of points at which the cost function is evaluated.

Equation equation (27) represent unconstrained nonlinear optimization problem, which is best suited for solving using evolutionary logarithms. It solved using MATLAB Genetic Algorithm (GA) method. The optimal 4-BM design vector is obtained as follows:

$$\chi = [51.4\ 31.2\ 28.3\ 55.0\ -23.9\ -4.0\ -0.31\ 2.66]^T \tag{28}$$

where angles are in radian and linear dimensions are in mm.

The optimal 4-BM yields a mean and maximum deviation of 0.23 mm and 0.55 mm, respectively.

Optimum Knee Hinge based on K-E CKC analysis

In this section, we present the optimal dimensional synthesis of two common polycentric knee hinges, namely geared and 4-BM knee hinges, To stress the need to minimize the maximum relative motion (linear and torsional) between the exoskeleton and the user thigh, the following cost function is used:

$$\begin{aligned} C_{hinge}(\chi) =& w_1 \max(|l_{kf} - l_{kf0}|) + \\ & w_2 \max(|\theta_{kf} - (\theta_{ef} - \alpha_{kf})|) \end{aligned} \tag{29}$$

where l_{kf0} is the value of l_{kf} at $\theta_{kf} = 0$; while w_1 and w_2 are weighting factors, which is chosen as $w_1 = 1$ and $w_2 = 5(180)/\pi$ to give the torsional deviation in degree five times the weight of linear deviation in mm.

Geared knee hinge: The design vector is selected to contain all the dimensions that affect the mechanism motion. The design vector can be presented as follows:

$$\chi = [O_{ez}\ O_{ey}\ \alpha_{e2}\ r_1\ r_3]^T \tag{30}$$

where the position of the hinge $(O_{ez}\ O_{ey})$ is measure relative to the $O_{k2}z_{k2}y_{k2}$ coordinate frame.

To ensure the obtained dimensions facilitate a compact and easily assembled design, the following constraints are formulated:

$$\begin{aligned} &-50mm \le O_{ez} \le 50mm; && 5mm \le r_1 \le 25mm \\ &-50mm \le O_{ey} \le 50mm; && 5mm \le r_3 \le 25mm \\ &-\pi \le \alpha \le \pi; && r_1 + r_3 \le 30mm \end{aligned} \tag{31}$$

The value of l_{kf} and θ_{kf} in the cost function (equation (29)) are obtained from equations (16) and (17). The constraints in equation (31) along with the cost function presented in equation (29) forms a nonlinear optimization problem with linear constrains.

4-BM knee hinge: To show the flexibility of our proposed design method, it is assumed a compact 4-BM knee hinge is needed. Thus constraints are imposed on the dimensions of the 4-BM linkage as follows:

$$30mm \leq l_{ei} \leq 45mm; \quad i = 1, 2, \ldots, 4 \tag{32}$$

The constrained presented in equation (32) besides the cost function stated in equation (29) define the design optimization problem.

The value of l_{kf} and θ_{kf} in the cost function equation (29) are obtained from equations (19), through (23).

Optimum knee hinge based on knee ICR

The same procedures used in finding the dimensions of the 4BM that replicate the knee motion are used to obtain the optimal dimension of a 4-BM knee hinge. In contrast to the method used to design the knee based on K-E CKC, here the knee hinge is designed using the traditional approach of replicating the human knee ICR. The cost function defined in equation (27) is used along with the constraints imposed on the dimension defined in equation (32) are used to formulate the optimization problem.

Simulation

The simulation tests the hypothesis that minimizing relative motion between the exoskeleton and the user is more crucial than replicating the knee ICR. The 4-BM knee model is simulated with different hinge designs using the proposed K-E CKC analysis. To ensure the comprehensiveness of the study, five hinge designs are used in this simulation, which are denoted as follows:

- **FC** Fixed center knee hinge design.
- **stGPC** Commercial polycentric geared hinge design.
- **opGPC** Optimized polycentric geared hinge design obtained based on K-E CKC analysis.
- **op4-BarPC** Optimized polycentric 4-BM hinge design obtained based on K-E CKC analysis.
- **opICRPC** Optimized polycentric 4-BM hinge design obtained based on replicating knee ICR.

The fixed center and the commercially available geared hinges are placed relative to the 4-BM knee model such that the hinge ICR is concentric with the knee model ICR at $\theta_{kf} = 0$.

To assess relative motion between the user's thigh and the knee brace/exoskeletons, the linear, Dev_L and torsional, Dev_θ deviations evaluated at point i are defined as follows:

$$Dev_L\,(i) = l_{kf}\,(i) - l_{kf0} \tag{33}$$

$$Dev_\theta\,(i) = \theta_{kf}\,(i) - (\theta_{ef} - \alpha_{kf}) \tag{34}$$

where l_{kf0} is the length of l_{kf0} at $\theta_{kf} = 0$.

Similarly, the maximum linear, $(Dev_L)_{max}$ and torsional, $(Dev_\theta)_{max}$ deviations are defined as follows:

$$(Dev_L)_{max} = \max|l_{kf} - l_{kf0}| \tag{35}$$

$$(Dev_\theta)_{max} = \max|\theta_{kf} - (\theta_{ef} - \alpha_{kf})| \tag{36}$$

The design vector for stGPC and opGPC hinges is defined in equation (30) while the design vector for op4-BarPC and opICRPC hinges is defined in equation (26). The optimum dimensional synthesis problem is implemented in MATLAB® and solved using the GA. The optimal dimensions vector, χ^* for the different optimized hinge designs are summarized in Table 1.

The design vector for the stGPC hinge is derived from the measured dimensions of commercially available geared knee braces. Assuming that the stGPC hing is perfectly aligned with the user's knee at $\theta_{kf} = 0°$, that yields the following:

$$\chi = \begin{bmatrix} I_{z0} & I_{y0} - 12.5 & \dfrac{\pi}{2} & 12.5 & 12.5 \end{bmatrix} \tag{37}$$

where I_{z0} and I_{y0} are the horizontal and vertical position of the knee ICR in mm relative to $O_{k2}z_{k2}y_{k2}$ at $\theta_{kf} = 0$.

In this simulation, the user's knee is modeled as a four-bar mechanism (4-BM) with dimensions derived from equation (28). This 4-BM knee model is then integrated with the five hinge designs.

Experiment

The experiment aims to evaluate the performance of the knee hinges designed using the proposed approach against the performance of the FC design. Consequently, two hinge designs—opGPC and FC—are being compared. The proposed method relies on an idealized model for the knee and the exoskeleton. The knee model presented in equation (1) is based on an average-sized knee, which may differ from that of a specific user. The experiment is conducted to validate the assumptions made in K-E CKC modeling; it seeks to assess how the opGPC design performs in typical practical situations. The experiment measures the relative motion between the knee brace and the user's thigh and investigates the possibility of brace migration.

Experimental procedures

Two identical commercial knee braces (Figure 6) were used to compare between the FC and opGPC hinges. The hinge of one of the braces was disassembled and replaced with the opGPC hinge, as shown in Figure 6b. The experiments were conducted in compliance with the protocol of the Ethics Committee of Harbin Institute of Technology. Before performing the experiments, the objective of this work, the experimental procedures, and the settings were explained to the subject. Written informed consent was obtained from the subjects for the publication of this study and any accompanying images. The subject was asked to perform four deep squats while wearing the brace with the FC hinge and then with the opGPC hinge.The subject manually adjusted the brace to ensure proper alignment at full extension and securely fastened it to minimize migration during the squat motion. Additionally, the subject was instructed to perform the motion at their normal speed and

Table 1. Optimal diminutions obtained using GA.

Design	χ^*
opGPC	$[17.6mm\ -8.6mm\ 1.7rad\ 16mm\ 14mm]^T$
op4-BarPC	$[34.38mm\ 38.01mm\ 34.56mm\ 45.0mm\ -25.84mm\ -10.86mm\ 0.06rad\ 0.69rad]^T$
opICRPC	$[41.27mm\ 33.12mm\ 30.00mm\ 45.00mm\ -24.06mm\ -4.22mm\ -0.27rad\ 2.67rad]^T$

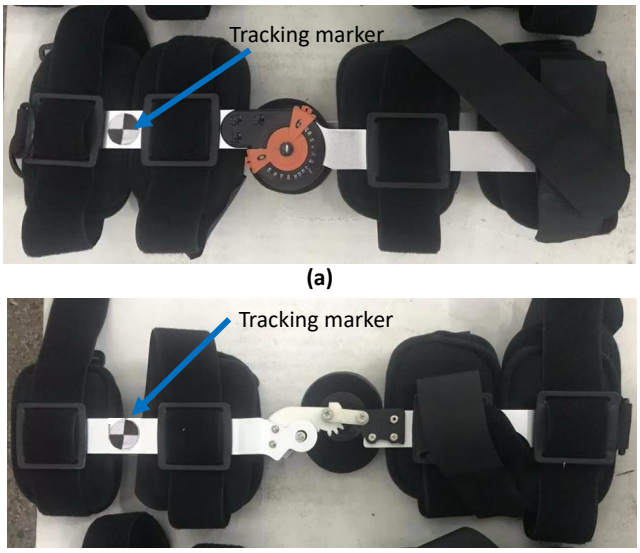

Figure 6. Knee braces used in the experiment with (a) FC hinge design, (b) opGPC hinge design.

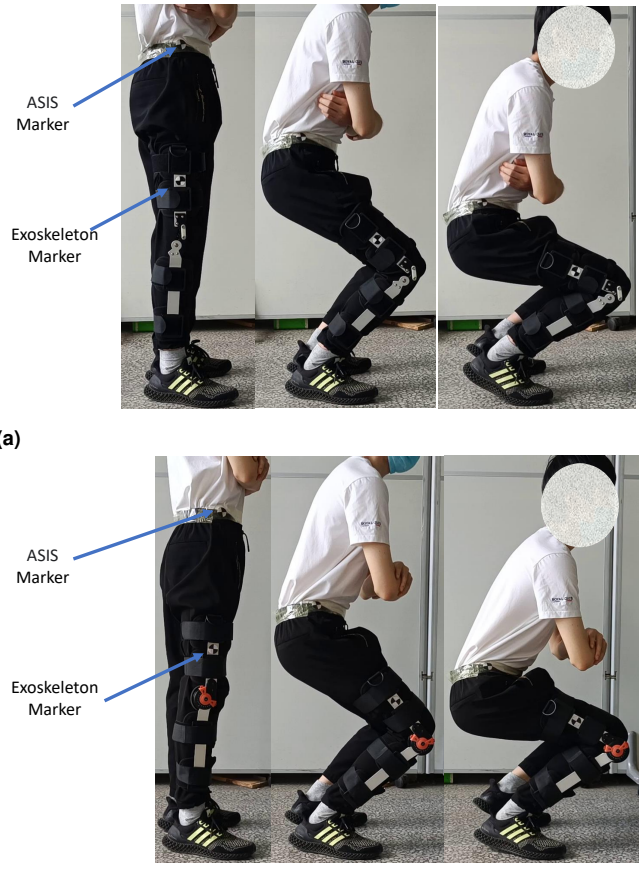

Figure 7. Snapshots of the subject performing a deep squat while wearing a knee brace with (a) opGPC hinge design, (b) FC hinge design.

to cross their arms over their chest to reduce the influence of arm movement during the experiment. Snapshots of the subject performing the deep squat while wearing opGPC and FC hinge designs are shown in Figures 7a and 7b, respectively. Two tracking markers were attached: one to the knee brace and another to the user's Anterior Superior Iliac Spine (ASIS), as illustrated in Figure 7. The two markers were tracked using a camera (1080p HD video recording at 60 fps, 48MP main sensor with sensor-shift OIS) fixed on a tripod, and the relative motions between the two markers were analyzed from the captured video using the Tracker video analyzing and modeling tool[40].

Results and discussion

The equations derived from the knee hinges are used to simulate the performance of different knee hinges as shown in Figure 8. The optimize hinges (opGPC, op4-BarPC and opICRPC) were able to follow the knee flexion with a small motion relative to the 4-BM knee model. The FC hinge shows appreciable deviation, which drastically increased with increasing the flexion angle. The stGPC hinge shows low deviation at low flexion angles but the deviation increases with increasing the flexion angle. This aligns well with the observation from Figure 1b and in[35]. Although opGPC and op4-BarPC hinges resulted in a different ICR than the typical human knee ICR shown in Figure 2b, the simulation shows that these hinges were able to follow the knee motion. The results indicate that reducing the relative motion between the exoskeleton and the user's thigh is more important in designing knee orthoses than following the knee ICR. This does not imply that the ICR is unimportant for other applications; it remains crucial to consider the ICR of prosthetic knee joints, as it significantly affects stability and the required hip extension-flexion moments for voluntary control of the prosthetic knee joint.[41].

To further investigate the capability of the proposed approach, different knee hinges were simulated under both perfect alignments (as shown in Figure 8a) and misalignment conditions (as shown in Figure 9b). In the perfect alignment scenario, the knee hinges were simulated without initial misalignment. In the misalignment scenario, the knee hinge was initially placed with a 10 mm offset in both horizontal and vertical directions relative to the perfect alignment case. Figure 9 shows that in both scenarios, the optimized knee hinges exhibit much lower linear and torsional deviations than the FC and stGPC designs. Although misalignment increases the linear and torsional deviations of the optimized hinges, these deviations remain significantly lower than those of the FC and stGPC designs. Comparing Figures 8 and 9a shows that while FC and stGPC designs have similar torsional deviations, the stGPC design experiences much lower linear deviation. This may explain why less relative motion is expected from the stGPC hinge compared to the

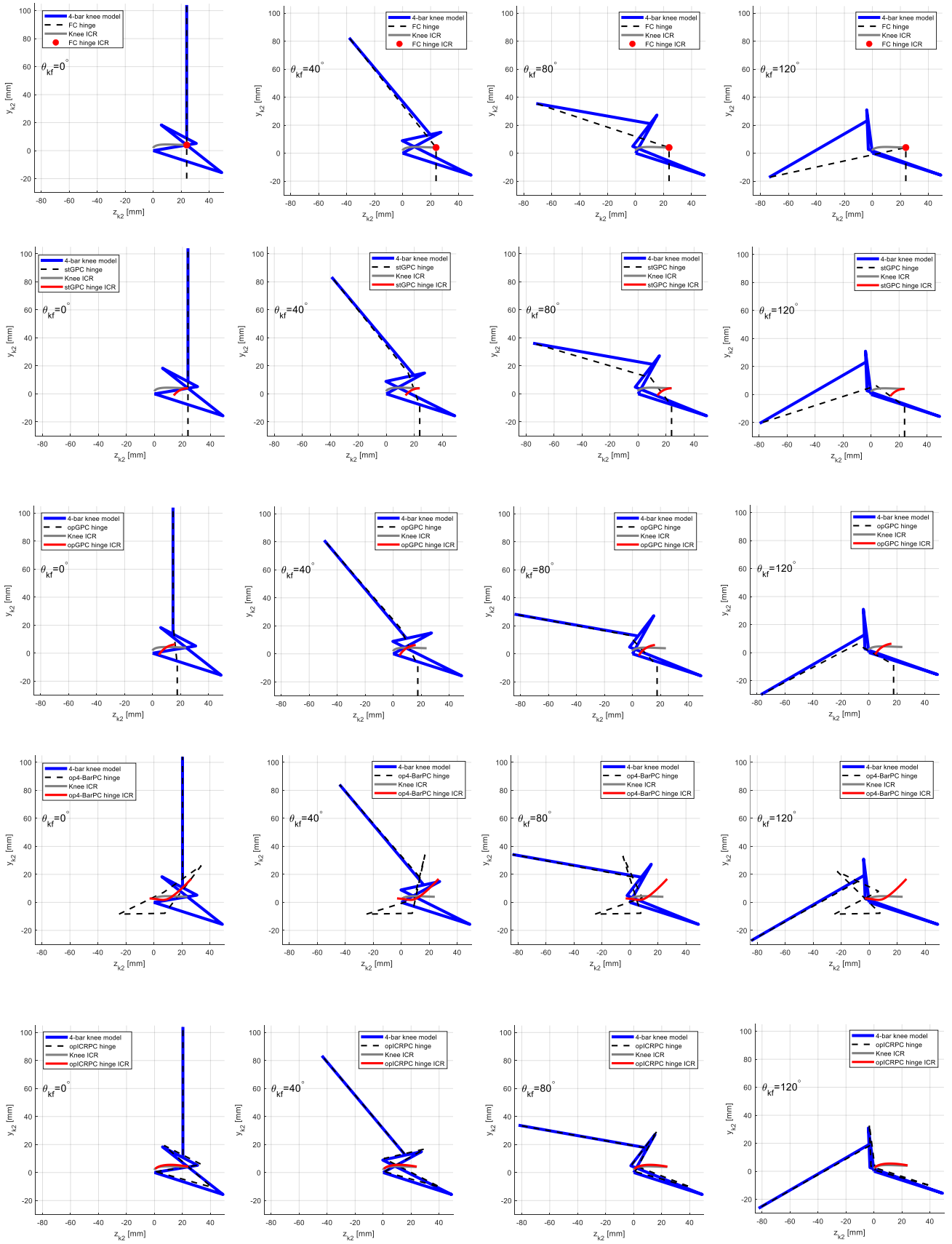

Figure 8. Simulation of the K-E CKC with FC, stGPC, opGPC, op4-BarPC and opICRPC hinges for $\theta_{kf} \in [0^\circ\ 40^\circ\ 80^\circ\ 120^\circ\ ]$.

FC hinge, especially at low flexion angles. The maximum linear and torsional deviations for the different hinge designs for both perfectly aligned (without offset) and misalignment scenarios for $\theta_{kf} \in [0 \quad 120^\circ]$ are summarized in Table 2.

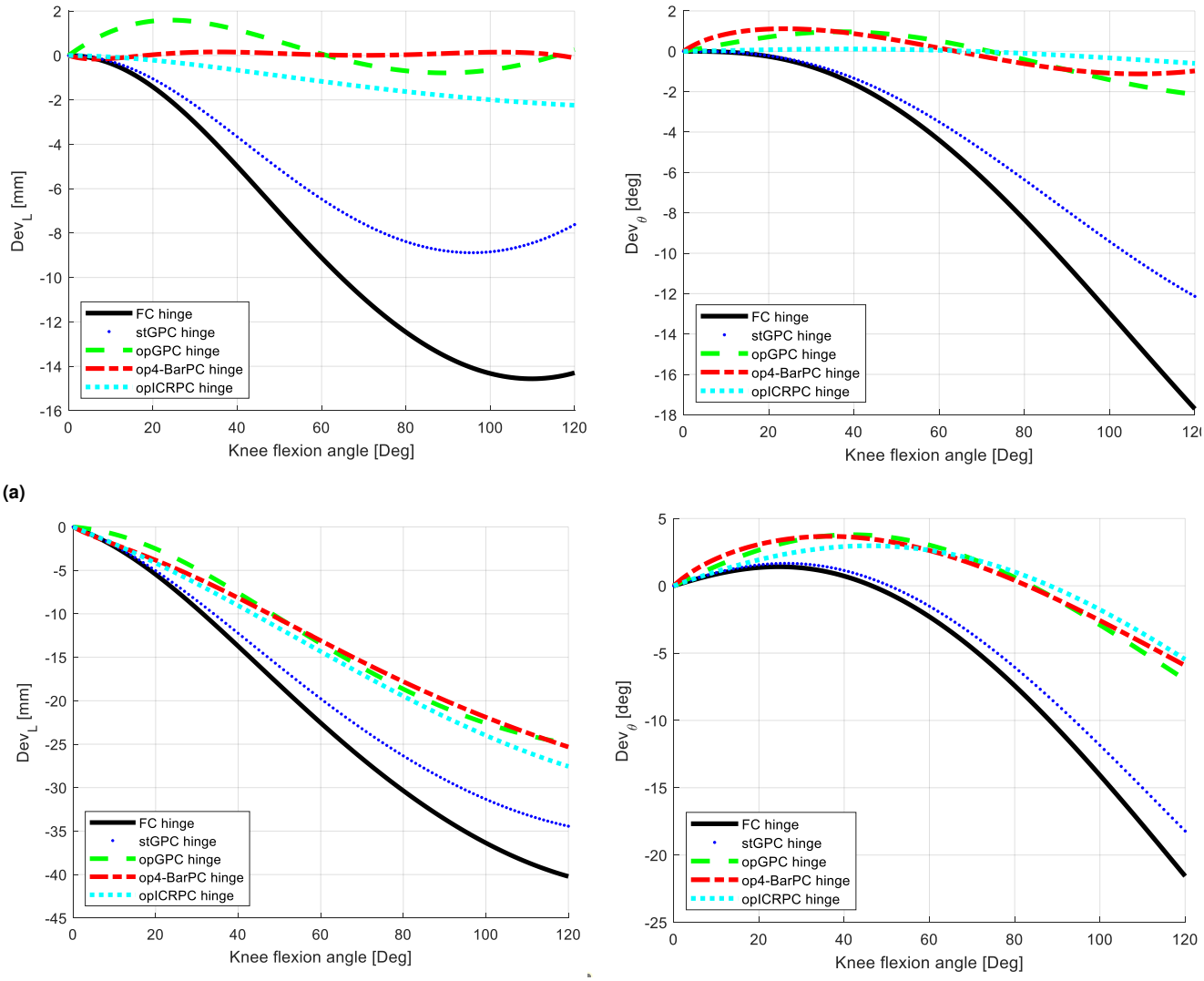

Figure 9. The linear deviation Dev_L and torsional deviation Dev_θ of K-E CKC for the different knee hinge designs, (a) without offset. (b) with offset.

The knee hinge design based on ICR (opICRPC) shows lower Dev_L and Dev_θ, which can explain why knee hinges designed using this approach receive good feedback from users[42]. It's important to note that the design based on ICR assumes perfect alignment and neglects the difference between the motion kinematics of the user's knee motion. The analysis of K-E CKC proposed in this paper provides a measure to quantify the relative motion between the user's thigh and the exoskeleton. Our preliminary studies and findings in the literature[35] indicate that the stGPC hinge satisfactorily follows knee motion at small flexion angles but begins to experience misalignment as the flexion angle increases. This trend is also captured by our proposed analysis, as shown in Figures 8 and 9.

The experimentally obtained changes in distance between the two markers for the FC and opGPC designs are shown in Figure 10. As expected from the simulation results, the distance change for the FC hinge design (Figure 10b) is significantly larger than for the opGPC hinge design (Figure 10a). Another feature evident in Figure 10b is the migration of the FC brace after two squats. In contrast, the opGPC design did not experience noticeable migration. Comparing the simulation results shown in Figure 9 with the experimental results in Figure 10 shows that the experiment yields a larger relative motion between the user's thigh and the brace than expected from the simulation. This could be due to the elasticity of the skin and soft tissues of the user's leg. Also, perfect alignment between the user's knee and brace joint can't be guaranteed in practice. As shown in Figure 8, a slight misalignment can greatly affect the relative motion between the exoskeleton and the user's knee. Despite that, the proposed model for K-E CKC was able to predict the general profile of the relative motion. Simulation results show that the proposed method can predict the relative motion between the user's thigh and knee hinge of different designs.Additionally, the experimentally observed increase in Dev_L and Dev_θ with knee flexion angle was predicted by our method.

Conclusions

A novel method has been developed to analyze and design knee exoskeletons that accommodate the complex motion of the human knee joint in the sagittal plane. The method

Table 2. The maximum linear and torsional deviations for the different hinge designs for both perfectly aligned (without offset) and misalignment scenarios.

Deaign	without offset		with offset	
	$(Dev_L)_{max}$ $[mm]$	$(Dev_\theta)_{max}$ $[^\circ]$	$(Dev_L)_{max}$ $[mm]$	$(Dev_\theta)_{max}$ $[^\circ]$
FC	14.56	17.71	40.22	21.57
stGPC	12.14	8.88	34.43	19.88
opGPC	2.38	3.1	24.90	10.77
op4-BarPC	0.32	2.24	25.32	9.60

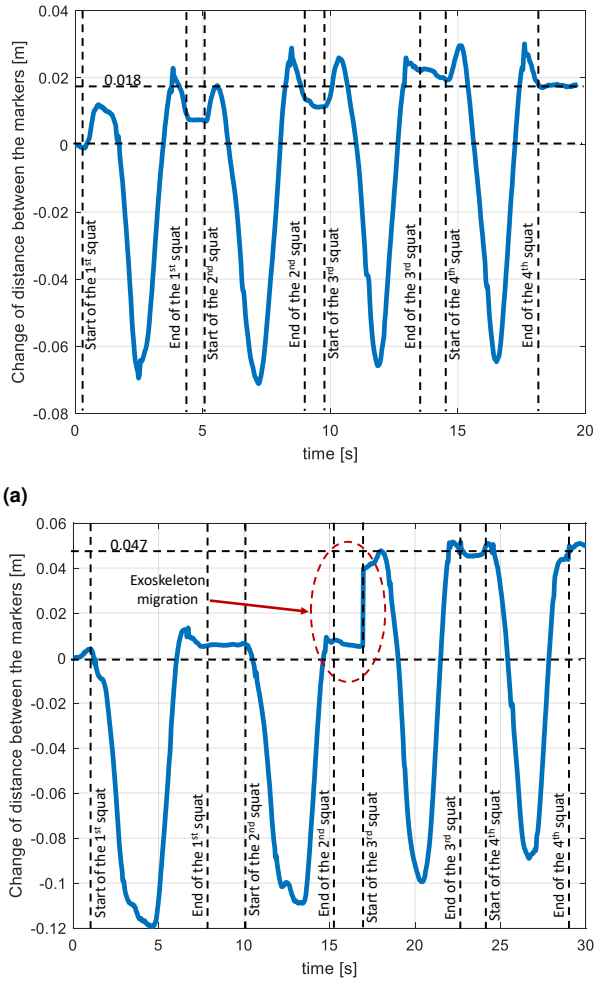

Figure 10. The change in the distance between the marker attached to the user and to the exoskeleton for four consecutive squats (a) opGPC hinge design, (b) FC hinge design.

proposes a 4-bar linkage as a model of human knee kinematics, which is integrated with a knee exoskeleton to create a closed-kinematic chain. The proposed method is suitable for evaluating the performance of different knee hinge designs by predicting the relative motion between the exoskeleton and the user's leg. The 4-bar knee model has been simulated with different hinge designs and alignment conditions to demonstrate the method's ability to assess movement relative to the user's leg. Furthermore, an experiment was conducted to compare the performance of a polycentric geared knee hinge, which is optimized using the proposed method, with that of a fixed center hinge. The results show that the optimized polycentric hinge reduces the relative motion between the exoskeleton and the user's leg while being less prone to exoskeleton migration. The simulation based on the proposed method has demonstrated a good correlation with the experimental results, specifically reflecting the trend of increased relative motion with an increasing flexion angle. The proposed method offers a simple and systematic approach to designing knee exoskeletons that provide a comfortable and safe interaction with the user.

References

1. Iwaki H, Pinskerova V and Freeman M. Tibiofemoral movement 1: the shapes and relative movements of the femur and tibia in the unloaded cadaver knee. *The Journal of Bone & Joint Surgery British Volume* 2000; 82(8): 1189–1195.
2. Smidt GL. Biomechanical analysis of knee flexion and extension. *Journal of biomechanics* 1973; 6(1): 79–92.
3. Asker A, Assal SF, Ding M et al. Experimental validation of a motion generation model for natural robotics-based sit to stand assistance and rehabilitation. In *2016 IEEE International Conference on Robotics and Biomimetics (ROBIO)*. IEEE, pp. 214–219.
4. Engebretsen L, Soligard T, Steffen K et al. Sports injuries and illnesses during the london summer olympic games 2012. *British journal of sports medicine* 2013; 47(7): 407–414.
5. Leyvraz P and Rakotomanana L. The anatomy and function of the knee–the quest for the holy grail?, 2000.
6. Nakagawa S, Kadoya Y, Todo S et al. Tibiofemoral movement 3: full flexion in the living knee studied by mri. *The Journal of Bone & Joint Surgery British Volume* 2000; 82(8): 1199–1200.
7. Mohamed AM and Sun R. A valid model for prediction tibiofemoral force for healthy people based on static optimization. *IEEE Access* 2021; 9: 88467–88477.
8. Nikolopoulos FP, Zacharaki EI, Stanev D et al. Personalized knee geometry modeling based on multi-atlas segmentation and mesh refinement. *IEEE Access* 2020; 8: 56766–56781.
9. Hill PF, Vedi V, Williams A et al. Tibiofemoral movement 2: the loaded and unloaded living knee studied by mri. *The Journal of Bone & Joint Surgery British Volume* 2000; 82(8): 1196–1198.
10. Karrholm J, Brandsson S and Freeman M. Tibiofemoral movement 4: changes of axial tibial rotation caused by forced rotation at the weight-bearing knee studied by rsa. *The Journal of Bone & Joint Surgery British Volume* 2000; 82(8): 1201–1203.
11. O'connor J, Shercliff T, Biden E et al. The geometry of the knee in the sagittal plane. *Proceedings of the Institution of Mechanical Engineers, Part H: Journal of Engineering in Medicine* 1989; 203(4): 223–233.
12. Pinskerova V, Maquet P and Freeman M. Writings on the knee between 1836 and 1917. *The Journal of Bone and Joint Surgery*

British volume 2000; 82(8): 1100–1102.
13. Smith PN, Refshauge KM and Scarvell JM. Development of the concepts of knee kinematics. *Archives of physical medicine and rehabilitation* 2003; 84(12): 1895–1902.
14. Goodfellow J and O'Connor J. The mechanics of the knee and prosthesis design. *The Journal of Bone & Joint Surgery British Volume* 1978; 60(3): 358–369.
15. Patel VV, Hall K, Ries M et al. A three-dimensional mri analysis of knee kinematics. *Journal of Orthopaedic Research* 2004; 22(2): 283–292.
16. Walker P, Kurosawa H, Rovick J et al. External knee joint design based on normal motion. *J Rehabil Res Dev* 1985; 22(1): 9–22.
17. Walker P, Rovick J and Robertson D. The effects of knee brace hinge design and placement on joint mechanics. *Journal of biomechanics* 1988; 21(11): 965–974.
18. Tucker MR, Shirota C, Lambercy O et al. Design and characterization of an exoskeleton for perturbing the knee during gait. *IEEE Transactions on Biomedical Engineering* 2017; 64(10): 2331–2343.
19. Gao M, Wang Z, Li S et al. Design and optimization of exoskeleton structure of lower limb knee joint based on cross four-bar linkage. *AIP Advances* 2021; 11(6).
20. Bertomeu JMB, Lois JMB, Guillem RB et al. Development of a hinge compatible with the kinematics of the knee joint. *Prosthetics and orthotics international* 2007; 31(4): 371–383.
21. Olinski M, Gronowicz A, Handke A et al. Design and characterization of a novel knee articulation mechanism. *International Journal of Applied Mechanics and Engineering* 3916; 21(3): 611–622.
22. Massardi S, Pinto-Fernandez D, Babič J et al. Relevance of hazards in exoskeleton applications: a survey-based enquiry. *Journal of NeuroEngineering and Rehabilitation* 2023; 20(1): 1–13.
23. Amigo LE, Casals A and Amat J. Design of a 3-dof joint system with dynamic servo-adaptation in orthotic applications. In *2011 IEEE International Conference on Robotics and Automation*. IEEE, pp. 3700–3705.
24. de Andrade RM, Fabriz Ulhoa PH, Fragoso Dias EA et al. Design and testing a highly backdrivable and kinematic compatible magneto-rheological knee exoskeleton. *Journal of Intelligent Material Systems and Structures* 2023; 34(6): 653–663.
25. Cempini M, De Rossi SMM, Lenzi T et al. Self-alignment mechanisms for assistive wearable robots: A kinetostatic compatibility method. *IEEE Transactions on Robotics* 2012; 29(1): 236–250.
26. Pott PP, Wolf SI, Block J et al. Knee-ankle-foot orthosis with powered knee for support in the elderly. *Proceedings of the Institution of Mechanical Engineers, Part H: Journal of Engineering in Medicine* 2017; 231(8): 715–727.
27. Brownstein B. Migration and design characteristics of functional knee braces. *Journal of Sport Rehabilitation* 1998; 7(1): 33–43.
28. Jarrassé N and Morel G. Connecting a human limb to an exoskeleton. *IEEE Transactions on Robotics* 2011; 28(3): 697–709.
29. Wang D, Lee KM, Guo J et al. Adaptive knee joint exoskeleton based on biological geometries. *IEEE/ASME transactions on mechatronics* 2013; 19(4): 1268–1278.
30. Celebi B, Yalcin M and Patoglu V. Assiston-knee: A self-aligning knee exoskeleton. In *2013 IEEE/RSJ International Conference on Intelligent Robots and Systems*. IEEE, pp. 996–1002.
31. Ergin MA and Patoglu V. A self-adjusting knee exoskeleton for robot-assisted treatment of knee injuries. In *2011 IEEE/RSJ International Conference on Intelligent Robots and Systems*. IEEE, pp. 4917–4922.
32. Jun S, Zhou X, Ramsey DK et al. Compliant knee exoskeleton design: Parallel coupled compliant plate (pccp) mechanism and pennate elastic band (peb) spring. In *International Design Engineering Technical Conferences and Computers and Information in Engineering Conference*, volume 46346. American Society of Mechanical Engineers, p. V003T12A006.
33. Zanotto D, Akiyama Y, Stegall P et al. Knee joint misalignment in exoskeletons for the lower extremities: Effects on user's gait. *IEEE Transactions on Robotics* 2015; 31(4): 978–987.
34. Asker A, Xie S and Dehghani-Sanij AA. Multi-objective optimization of force transmission quality and joint misalignment of a 5-bar knee exoskeleton. In *2021 IEEE/ASME International Conference on Advanced Intelligent Mechatronics (AIM)*. IEEE, pp. 122–127.
35. Patrick S, Anil Kumar N and Hur P. Evaluating knee mechanisms for assistive devices. *Frontiers in Neurorobotics* 2022; 16: 790070.
36. Cai D, Bidaud P, Hayward V et al. Design of self-adjusting orthoses for rehabilitation. In *Proceedings of the 14th IASTED International Conference Robotics and Applications*, volume 74.
37. Cai VAD, Bidaud P, Hayward V et al. Self-adjustment mechanisms and their application for orthosis design. *Meccanica* 2017; 52: 713–728.
38. Bapat GM and Sujatha S. A method for optimal synthesis of a biomimetic four-bar linkage knee joint for a knee-ankle-foot orthosis. In *Journal of Biomimetics, Biomaterials and Biomedical Engineering*, volume 32. Trans Tech Publ, pp. 20–28.
39. Asker A and Assal SF. Kinematic analysis of a parallel manipulator-based multi-function mobility assistive device for elderly. In *2015 IEEE International Conference on Advanced Intelligent Mechatronics (AIM)*. IEEE, pp. 676–681.
40. Brown D. Tracker free video analysis and modeling tool for physics education. Retrieved from https://physlets.org/tracker/, 2012.
41. Soriano JF, Rodríguez JE and Valencia LA. Performance comparison and design of an optimal polycentric knee mechanism. *Journal of the Brazilian Society of Mechanical Sciences and Engineering* 2020; 42: 1–13.
42. Tucker MR, Moser A, Lambercy O et al. Design of a wearable perturbator for human knee impedance estimation during gait. In *2013 IEEE 13th International Conference on Rehabilitation Robotics (ICORR)*. IEEE, pp. 1–6.